Hydrogen Chemical Configuration and Thermal Stability in Tungsten Disulfide Nanoparticles Exposed to Hydrogen Plasma

Alex Laikhtman*[1], Gennady Makrinich[1], Meltem Sezen[2], Melike Mercan Yildizhan[2], Jose I. Martinez[3], Doru Dinescu[4], Mariana Prodana[4], Marius Enachescu[4], Julio A. Alonso[5], Alla Zak*[1]

[1]*Sciences Department, Holon Institute of Technology (HIT), 52 Golomb St., Holon, 5810201 Israel*

[2]*Sabanci University Nanotechnology Research and Application Center (SUNUM), Orhanli, Tuzla, 34956 Istanbul, Turkey*

[3]*Department of Surfaces, Coatings and Molecular Astrophysics, Institute of Material Science of Madrid (ICMM-CSIC), Sor Juana Inés de la Cruz 3, 28049 Madrid, Spain*

[4]*Center for Surface Science and Nanotechnology (CSSNT), University Politehnica of Bucharest, Splaiul Independentei 313, 060042 Bucharest, Romania*

[5]*Department of Theoretical, Atomic and Optical Physics, University of Valladolid, 47011 Valladolid, Spain*

*Corresponding authors. E-mails: alexl@hit.ac.il, alzak@hit.ac.il

Abstract

The chemical configuration and interaction mechanism of hydrogen absorbed in inorganic nanoparticles of WS_2 are investigated. Our recent approaches of using hydrogen activated by either microwave or radiofrequency plasma dramatically increased the efficiency of its adsorption on the nanoparticles surface. In the current work we make an emphasis on elucidation of the chemical configuration of the adsorbed hydrogen. This configuration is of primary importance as it affects its adsorption stability and possibility of release. To get insight on the chemical configuration, we combined the experimental analysis methods with theoretical modeling based on the density functional theory (DFT). Micro-Raman spectroscopy was used as a primary tool to elucidate chemical bonding of hydrogen and to distinguish between chemi- and physisorption. Hydrogen adsorbed in molecular form (H_2) was clearly identified in all the plasma-hydrogenated WS_2 nanoparticles samples. It was shown that the adsorbed hydrogen is generally stable under high vacuum conditions at room temperature, which implies its stability at the ambient atmosphere. A DFT model was developed to simulate the adsorption of hydrogen in the WS_2 nanoparticles. This model considers various adsorption sites and identifies the preferential locations of the adsorbed hydrogen in several WS_2 structures, demonstrating good concordance between theory and experiment and providing tools for optimizing of hydrogen exposure conditions and the type of substrate materials.

Introduction

The use of hydrogen in the renewable energy systems requires an effective, safe, and stable storage solution. Nanostructured materials such as inorganic nanotubes (INT) and inorganic fullerene-like (IF) nanoparticles (NP) are appealing because of their extremely high surface area and layered structure, where potentially many sites can either chemi- or physisorb hydrogen. A newly developed technology enables the synthesis and production of pure IF and INT phases of WS_2 in commercial quantities.[1,2] Therefore, WS_2 INT and IF have been tested as possible candidates for hydrogen storage material with a significant industrial potential. These materials may allow hydrogen to be either chemi- or physisorbed inside their crystalline structure, inside hollow cores of IF/INT, on their surface or in the open interstitial pore spaces of IF/INT powder meshes. Recently, exposure to high pressure molecular hydrogen at 35-350 °C was found to have measurable but limited adsorption rate - up to 0.2 wt.% of hydrogen.[3] This approach to use plasma activated hydrogen successfully resulted in significant increase of the hydrogen adsorption concentration. Indeed, treatment of the WS_2-INT and WS_2-IF by hydrogen activated in microwave (MW) plasma resulted in much higher values of the adsorbed hydrogen content, ~1 wt.%.[3] This enhancement in the hydrogen adsorption concentration was attributed to more effective interaction of plasma-activated *vs.* high pressure molecular hydrogen with NP substrate surfaces. The increase of hydrogen adsorption was due to the stronger chemisorption of the atomic/ionized hydrogen formed in the MW plasma compared to weaker physisorption of molecular hydrogen, and to higher energy and momentum of the hydrogen molecules in the plasma environment. In addition, plasma-originated hydrogen ions and electrons may interact with the WS_2 NP modifying existing defects and pores, or producing new ones, and so contribute to hydrogen binding, diffusion, and higher stability of its adsorption. An important consideration for choosing low energy hydrogen plasma as the activation method was in the high permeation of hydrogen/deuterium combined with the retention of the plasma properties along sample width. It was shown that hydrogen and deuterium molecules keep their highly vibrational excited states while passing from the outermost nanoparticles in the web to the innermost ones.[4-6] This process should guarantee that most of the NP in the powder batch face similarly excited hydrogen molecules and undergo the same plasma treatment. This phenomenon is of particular importance ensuring homogeneous distribution of the adsorbed hydrogen through the exposed powder samples.

High hydrogen concentrations in the materials, proposed as media for hydrogen storage, is an important task, together with appropriate storage and release properties. However, these goals could be successfully accomplished only if the adsorption mechanism, chemical configuration and energy states of the adsorbed hydrogen are well understood. INT and IF of WS_2 provide excellent tools for such a study owing to their simple structure, chemical and thermal stability, ease of modeling of their interaction with hydrogen molecules and ions, and possibility of precise calculation of the energy states of variously adsorbed species. The main novelty of this work is getting insight on the chemical configuration, by combination of experimental analysis methods and theoretical modeling. Our primary goal was to study the chemical configuration of the adsorbed hydrogen and to elaborate on its thermal stability inside the WS_2 NP (either IF or INT) under ambient conditions. Whereas actual optimization of the technical parameters aiming to further increase the hydrogen adsorption rate in these specific materials is left out of the scope of the present work. A number of experimental techniques were applied for this purpose. Micro-Raman spectroscopy was extensively used to evaluate the chemical configuration of hydrogenated compounds due to its capability to detect chemical bonds involving hydrogen atoms.[7-10] This method was highly sensitive and allowed to discover molecular hydrogen inside amorphous and crystalline solids.[10] In addition, we used plasma of deuterium instead of hydrogen in several experiments to unambiguously prove that the measured features are due to the hydrogenation (deuteration) by plasma and not due to residual water or hydrogen retained from the synthesis of WS_2 NP. Precise and well explained data for micro-Raman spectra of different types of WS_2 NP has been recently reported.[11,12] Transmission electron microscopy (TEM) analysis of NP after plasma treatment was used to accurately examine the pristine changes on the NPs' surface and in their interlayer distances. To study the interaction of the INT-WS_2 and IF-WS_2 with activated H_2 we also monitored them by electron diffraction (ED), and X-ray diffraction (XRD).

High thermal stability of the substrate materials (NP of WS_2)[13] allowed us to carry out thermogravimetric analysis (TGA) aiming to determine the weight percent and thermal stability of the adsorbed hydrogen.

A DFT model specifically developed for these WS_2 NP materials was applied for the first time to calculate the energy of different adsorption sites and thus to determine the actual configuration of adsorbed hydrogen/deuterium.

Experimental

The IF-WS_2 and INT-WS_2 were synthesized from tungsten oxides by solid-gas reaction via the combined reduction-sulfidization process, at elevated temperatures of 750-900 °C, as it was described in detail elsewhere.[2,14,15] This process, first, leads to the formation of the external cylindrical/spherical sulfide layer on the surface of the oxide whiskers/spherical NP, and then, to outwards-inwards gradual sulfurization of the oxide core resulting in hollow multiwall WS_2-INT NP. The studied nanotubes were of 50-150 nm wide and ~20 μm long, and semi-spherical WS_2-IF NP- of 50-250 nm in diameter.

Exposure of the WS_2 NP to hydrogen/deuterium activated by radiofrequency (RF) plasma was performed in the plasma reactor dedicated to this purpose. The pure IF-, pure INT-WS_2, and a ~1:1 mixture of INT with bulk WS_2 platelets, in the form of either powder or a pressurized tablet ~70 mg each, were used as substrate materials for the RF hydrogen plasma treatment. Before the exposure to plasma, the substrate materials were *in situ* annealed at 300 °C for ~15 min (or until the pressure decreased to the initial value - prior to the annealing) in high vacuum (base pressure $<2\times10^{-5}$ Torr) to remove residual water and other contaminations. After cooling down to room temperature, the powders or the tablet were cleaned for 10 min by 200 W Ar plasma. This value of plasma power does not affect the structure of the WS_2 NP, as it was previously reported for even higher Ar plasma power values (up to 400 W).[16] After this cleaning procedure, the WS_2 substrates were immersed into a RF plasma of either hydrogen or deuterium. The 400 W power RF plasma of hydrogen or deuterium was maintained during 30 min under gas pressure of 1 Torr, which resulted in minor temperature increase up to 35 °C. Later on the powders were evacuated from the plasma reactor chamber for different analyses. However, to evaluate the success of the hydrogenation process and to find the optimal conditions for the RF plasma, several sets of the hydrogenated/deuterated samples were *in situ* annealed and the relative pressure changes were measured as a function of the annealing temperature. This is unlike MW plasma hydrogenation previously reported,[3] where the *in situ* pretreatment and post-treatment annealing were not possible.

To determine the chemical nature of hydrogen adsorbed in the NP as a result of the plasma treatment, micro-Raman measurements were performed in either Horiba LabRam 800 (CSSNT) or Renishaw InVia (SUNUM) microspectrometers. The Horiba instrument was particularly suitable as it is capable to measure

spectral features in a range of up to 5000 cm^{-1}. The green laser light of 532 nm was used for excitation being focused to a spot of 1-3 μm in diameter. Special precautions, like performing the measurements under continuous flow of nitrogen gas and limiting the laser power to <300 μW, were undertaken to prevent material heating under the laser beam,[17] but it was not possible to fully avoid it. This could result in partial desoprtion of H_2 under laser irradiation. Moreover, some oxidation of the substrate material was observed when irradiated for a longer time at higher laser intensities. For all substances the non-hydrogenated samples, used as references, were measured as well.

To elucidate the thermal stability of the adsorbed hydrogen and to determine its concentration, TGA measurements in a He atmosphere were performed in the temperature range of 25-500 °C using the SDT Q600 Simultaneous TGA/ DSC instrument.

To compare the morphological and structural quality of the materials before and after their treatment with hydrogen/deuterium plasma, TEM, and XRD measurements were carried out. ED pattern in the TEM was used to determine the evolution of the inter-planar spacing in the WS_2 NP as a result of hydrogen/deuterium adsorption. For the TEM investigations, a JEOL ARM 200F TEM/STEM system was used.

With the exception of the *in situ* pressure measurements, all other analysis techniques were performed *ex situ*~~., meaning that the NP of the upper most layer facing the plasma flux were homogeneously mixed with the deeper lying NP.~~

Results and Discussion

Plasma induced hydrogen adsorption and thermal stability

As explained above, to evaluate the success of the RF plasma hydrogenation/deuteration process one set of the samples was heated at a rate of ~20 °C/min to release the adsorbed gases at the end of the hydrogenation process and after gas evacuation. The pressure vs temperature dependence was recorded. In Figure 1 the results obtained for WS_2-IF and WS_2-INT, 30 min and 5 h after hydrogenation and deuteration, as well as the reference measurement of the empty plasma chamber are shown. The curves were normalized to the average sample mass of 60 g. Indeed, as seen from this figure the pressure increased even after

deducting the pressure increase measured for the same experimental setup and after hydrogen plasma treatment, but without any substrate material (line 1). In such a way, the obtained pressure increase was entirely attributed to hydrogen release from the plasma-exposed WS_2 NP and originates from this plasma-hydrogenation process only. For lines 2 and 6 two distinct peaks were observed for the samples measured within 30 min after plasma treatment, at 38 °C and around 80 °C. The pattern of the lines 4 and 5 is more complex as a result of lower intensity of the second (higher temperature) peak. The first feature (at the lower temperature) could be attributed to weekly bonded hydrogen, probably located on the surface, and the second one (at the higher temperature) is due to release of more strongly bound or deeper lying hydrogen. The relative amounts of released hydrogen were qualitatively compared by integration of the curves areas for the entire temperature range, estimated as 1:0.8:0.95:0.65:0.75for lines 2-6, respectively. It can be observed that the most substantial integral pressure increase was obtained for the deuterated and hydrogenated IF (lines 2 an 4). The curves for all the samples measured within 30 min revealed maximum hydrogen release at ~38-40 °C, while the peak obtained for IF is higher compared with the peak for INT. However, the release of deuterium from the INT was slower and the integrated area under the curve is not much slower than for IF. For all materials, the pressure started to grow (i.e., hydrogen started to desorb) at ~ 34 °C, while different temperatures as high as 300 °C were required to entirely release of all plasma-adsorbed hydrogen for various samples. It should be noted, however, that the measured temperature response to the heating was somewhat different between various samples due to some variations in their masses, grains sizes and the structures.

To elaborate on the stability of the plasma-adsorbed hydrogen or deuterium, the pressure increase upon heating was measured at the delay of 5 h after deuteration (Figure 1, line 3). The fact that most of D_2 remained adsorbed and then released even after 5 h of vacuum storage, following the exposure process, is indicative on its high adsorption stability. The relative deuterium concentrations (total area under the curves) remained quite similar for the 30 min (line 2) as for 5 h delay (line 3): 1:0.8, respectively, although the onset of desorption shifted from 34 °C to 46 °C and the desorption rate was slower. In agreement with our previous assumption, this small but measurable hydrogen loss during the 5 h-delay vacuum storage, which is reflected in the shift in the onset temperature, can be attributed to desorption of non-bonded hydrogen molecules, probably on the very surface of the NP under continuous pumping in the chamber.

It is stressed that numerous adsorption-desorption cycles were performed and only negligible differences were recorded between the cycles.

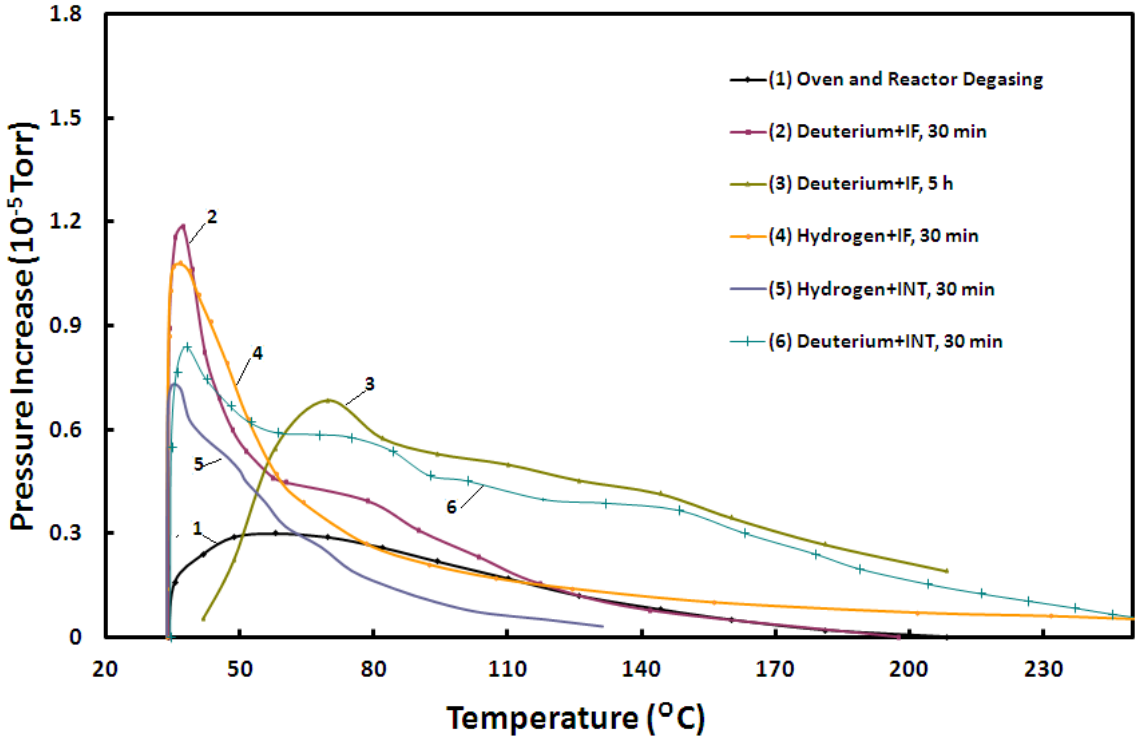

Figure 1. Heating-induced pressure increase of the RF plasma hydrogenated and deuterated WS_2 NP.

One would like to integrate the pressure curves in Figure 1, by converting the pressure data to the mass flow, to determine absolute hydrogen concentrations in our WS_2 materials. However, the large volume of the chamber (> 100 lit), constant flow of hydrogen and pumping during the measurements, the position of the pressure gauge far from the sample, along with unknown hydrogen desorption kinetics, and somewhat non-homogeneous temperature response make these calculations inaccurate. As an alternative method for quantitative measurements of adsorbed hydrogen, the TGA was subsequently performed. The results of the TGA measurements for untreated (as synthesized) and hydrogenated INT-WS_2 are presented in Figure 2 (lines 1,2). It can be observed that the reference sample lost more weight during the heating than the hydrogenated one. However, the desorption peak of the former appears just above 120 °C as seen from the derivative curve 2' which, therefore, is attributed to evaporation of the residual water mostly and is consistent with previously reported TGA data.[13] The maximum rate of the weight loss for the hydrogenated sample was obtained at 80 °C, as evident from the derivative curve 1', which is at a similar position to the

second peak (~80 °C) in the pressure measurements presented in Figure 1. It can be attributed to the adsorbed hydrogen. The absence of the peak associated with water desorption (120 °C) for the hydrogenated sample is not absolutely clear yet, since TGA measurements were performed *ex situ*, when both samples were exposed to air. We can only suggest at this point that WS_2 NP gained hydrophobic properties by the fact that adsorbed hydrogen prevents water molecules from sticking the NP surface.

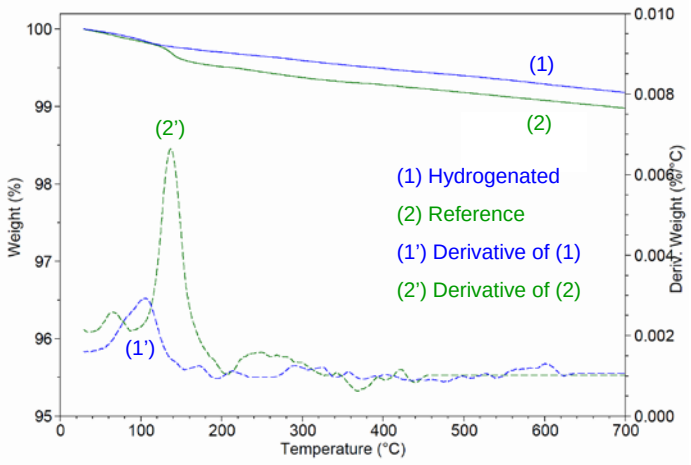

Figure 2. TGA plots (lines 1,2) for reference (green line) and hydrogenated (blue line) WS_2 NP. The appropriate derivative curves (lines 1',2') are plotted below.

The hydrogen concentrations estimated from TGA curves measured for all hydrogenated samples (not shown), were in the range of 0.4-0.55 wt. %. This value is more than twice the values measured for the WS_2 materials exposed to unactivated high pressure hydrogen, as reported in our previous work, though lower than for the WS_2 NP hydrogenated by MW plasma.[3] We would like to stress again that the analysis methods of the MW plasma hydrogenated samples were completely different from those used in this study, which makes the comparison of the results not simple. In addition, in the MW plasma reactor the *in situ* measurements of hydrogen release were not technically possible.

For the deuterated samples, the TGA measurements showed nearly identical behavior as for hydrogenated WS_2, and the estimated mass concentration of the plasma-adsorbed deuterium was about twice that of hydrogen, as the ratio of their molecular masses. This result confirms that released H_2 is due to the initial hydrogenation and not because of the H_2 residuals from the synthesis reaction, assuming that the

amount of the adsorbed D_2 and H_2 molecules was the same under similar plasma conditions for the same type of WS_2 NP.

It should be emphasized that the TGA measurements were performed *ex situ*, several days or weeks after the plasma-hydrogenation process, while the samples were stored at ambient atmosphere in closed vials. Therefore, we suppose that the real hydrogen concentration adsorbed by the samples immediately after plasma treatment is somewhat higher than the values listed above.

As evident from the results presented in Figure 1 and those of TGA, various types of WS_2 NP adsorb somewhat different quantity of hydrogen or deuterium. We leave the explanation of this aspect for our future work and concentrate here on the chemical configuration of the adsorbed hydrogen/deuterium.

Determination of chemical configuration of plasma-adsorbed hydrogen/deuterium

To determine the chemical configuration of the adsorbed hydrogen, micro-Raman measurements were performed. The laser induced heating accounted for a significant problem, as it could result in immediate desorption of hydrogen from the irradiated area and oxidation of WS_2. In the previous study of one of us,[17] the temperatures in excess of 1000 °C were measured on the microcrystalline particles under the micro-Raman laser spot of the power similar to the values used in the current work. These results were obtained when heat dissipation mechanism was ineffective. Indeed using the laser power above 0.3 mW focused to the spot of ~1 μm resulted in oxidation of the studied materials as evidenced by strong W-O Raman peaks at ~900 cm^{-1} (data not shown),[18] and visual color change (from brown-black to greenish-yellow) of the laser-irradiated area. It was shown previously that the oxidation process of WS_2 NP occurs in air at the temperatures >300 °C.[13] The oxidation of NP confirms that the temperature of the NP probed by the micro-Raman laser beam increased to >300 °C. At these conditions the hydrogen desorption is inevitable, as clear from Figure 1. In order to prevent or diminish these disturbances, a low laser power was used. However, this unfavorably affected the quality of the recorded spectra, bearing in mind a very low cross section of the Raman features related to molecular hydrogen.[19,20]

The micro-Raman scattering for all samples was measured in the spectral range of 0-4400 cm^{-1}. The typical result obtained for both virgin and hydrogenated INT-WS_2 in the window of 0-1200 cm^{-1} is depicted in Figure 3. Two characteristic modes of WS_2 can be clearly observed: the E_{2g} mode at 356 cm^{-1} and the A_{1g}

mode at 419 cm^{-1}. This spectrum resembles those previously measured for our substrate materials and described in great detail elsewhere.[13,14]

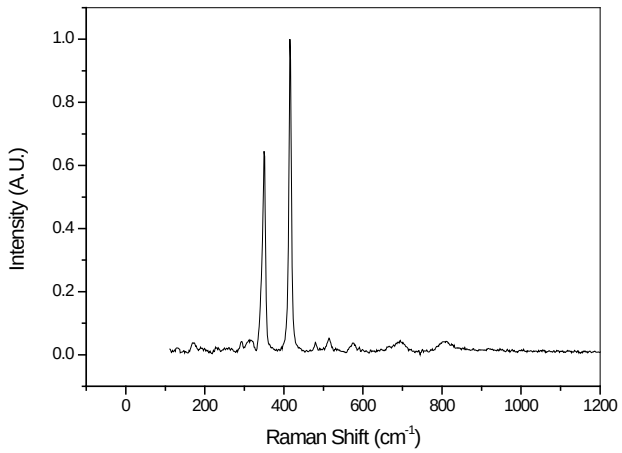

Figure 3. The typical micro-Raman spectrum measured for WS_2 NP. No change following the hydrogenation was observed in this spectral region.

A narrower spectral region of 3400-4300 cm^{-1} for the hydrogenated NP of each type was measured and similar results were obtained for all types of the WS_2 NP. As before, the micro-Raman spectra of reference, non hydrogenated materials were also recorded. In Figure 4 the spectra for the INT mixed with bulk WS_2 are presented. A small peak centered at ~4150 cm^{-1} was observed for the hydrogenated samples only (line 2). This peak was the most prominent for the 1:1 mixture of the INT with bulk NP, the intermediate intensity was recorded for the IF-WS_2, and the lowest though still measurable feature was observed for the pure INT-WS_2. This feature was previously attributed to the H–H stretching mode in H_2 molecules,[10,19,20] and, therefore, its appearance in our spectra reveals that indeed hydrogen adsorption took place and is present in the molecular (H_2) form. One should take into account a very small Raman cross section of this H-H mode as compared to the Raman peaks of WS_2 and a strong fluorescence background above 3000 cm^{-1}. We may suppose that H_2 molecules were adsorbed on the surface of the NT, in the hollow core or being intercalated between the layers in the WS_2 NP of all types.

To finally prove that the Raman feature measured at 4150 cm^{-1} is indeed due to physisorbed H_2 molecules, the sample was heated in vacuum to 450 ºC for several discrete periods lasting between 15 min to 2 h. The intensity of the H_2 mode peak gradually decreased until nearly disappeared following the longest annealing time, as shown in the Figure 4 (line 3).

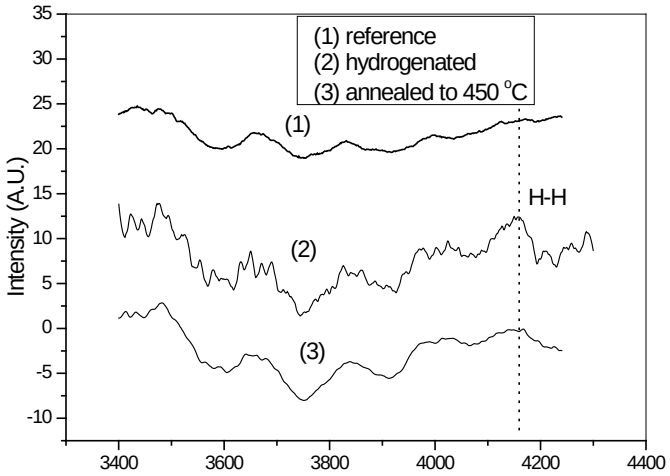

Figure 4. Micro-Raman spectra of WS_2 NP zoomed to the 3400-4300 cm^{-1} region: (1) reference (non-hydrogenated), (2) RF-plasma hydrogenated, (3) RF-plasma hydrogenated, then vacuum annealed at 450 °C.

To determine the presence of chemisorbed hydrogen (H-S bonding) Raman scattering measurements were performed in the 1500–3000 cm^{-1} region (not shown). However, the features which could be attributed to H-S bonds[21] never appeared, so indicating that no chemisorbed hydrogen was present in the WS_2 NP, at least at the moment of performing the Raman measurements. Nevertheless, we suspect that atomic hydrogen or free hydrogen ions, which could adsorb or intercalate in between the layers of WS_2 structure and create chemical bonds on the open edges or defects, desorbed as a result of environmental interaction, similar to that observed previously.[22] Additional study is required to clarify this aspect.

Nevertheless, to unambiguously prove that micro-Raman spectroscopy is indeed capable to reveal molecular hydrogen in WS_2, the deuterium gas in the RF plasma was used instead of hydrogen. To determine the chemical configuration of the adsorbed deuterium, micro-Raman measurements were performed in the spectral range of 2500-4000 cm^{-1}, and the results are shown in Figure 5. Indeed, a small peak, now centered at ~2970 cm^{-1} was observed (Figure 5, line 1). This feature was previously attributed to the D–D stretching mode in deuterium (D_2),[19,23] and, therefore, its appearance in our spectra proves that deuterium is present in the molecular form as was in the case of hydrogen. No features related to D-S bonds

were observed here too.[24,25] Furthermore, RF plasma deuterated WS_2 samples (IF and INT) were heated in vacuum to 450 ºC for up to 120 min, as for the hydrogenated samples. As seen from Figure 5 (line 2), the intensity of the ~2970 cm^{-1} peak decreased to nearly zero, supporting our assumptions that the observed mode corresponds to adsorbed D_2 gas.

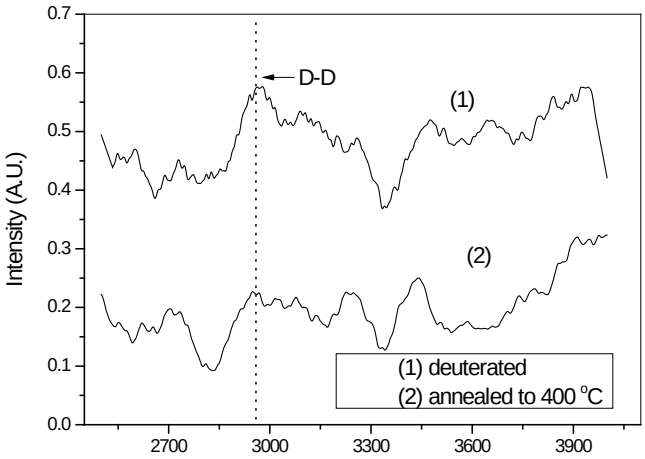

Figure 5. Micro-Raman spectra of (1) deuterated and (2) subsequently vacuum-annealed WS_2 NP.

The XRD spectra (data not shown), did not show measurable changes in the crystalline structure after RF hydrogen plasma treatments. This evidence is indicative of stability of the tubular and fullerene-like structures under plasma treatment. On the other hand, it is illustrative of the absence of systematic hydrogen intercalation in between the layers of WS_2 samples. Nevertheless, the high resolution TEM image of the plasma-hydrogenated IF-NP depicted in Figure 6 shows that in some particles the interlayer distance was increased to more than 0.65 nm (up to 0.85 nm in a few isolated locations, shown by arrows) as compared to the 0.62 nm interlayer distance in the non-affected regions. This expansion was not observed in pristine NP but did occur in WS_2 NP intercalated by foreign species.[22] The ED pattern on the individual NP is also shown in Figure 7, confirming the expansion of the layers from 0.62 nm (3.22 1/nm) for the unexposed NP to 0.65 nm (3.09 1/nm) for the hydrogenated NP. The difference between XRD and TEM/ED data could be due to the sampling features used in both techniques, namely large amount of powder used in XRD gives average spectra from many NP, while TEM and ED analyze an individual NP. As a consequence, we suppose that not all NP or/and not all the layers were expanded. The intercalation of hydrogen between the WS_2 layers can be the natural explanation for this expansion. The dynamics of layers expansion in intercalated WS_2 NP stored in ambient conditions was previously discussed.[22] ~~It was shown that~~

~~intercalation of the light ions/atoms, like Na and K does not result in the expansion of the layers (due to the electrostatic interaction) until the adsorption of water molecules from air, attracted by intercalated atoms, occurs. Moreover, storage of the samples in ambient conditions resulted in de-intercalation and shrinking back of the layers. Therefore, occasional observation of the expanded layers in the hydrogenated samples discussed in this work could be attributed to the de-intercalation as a result of aging~~.

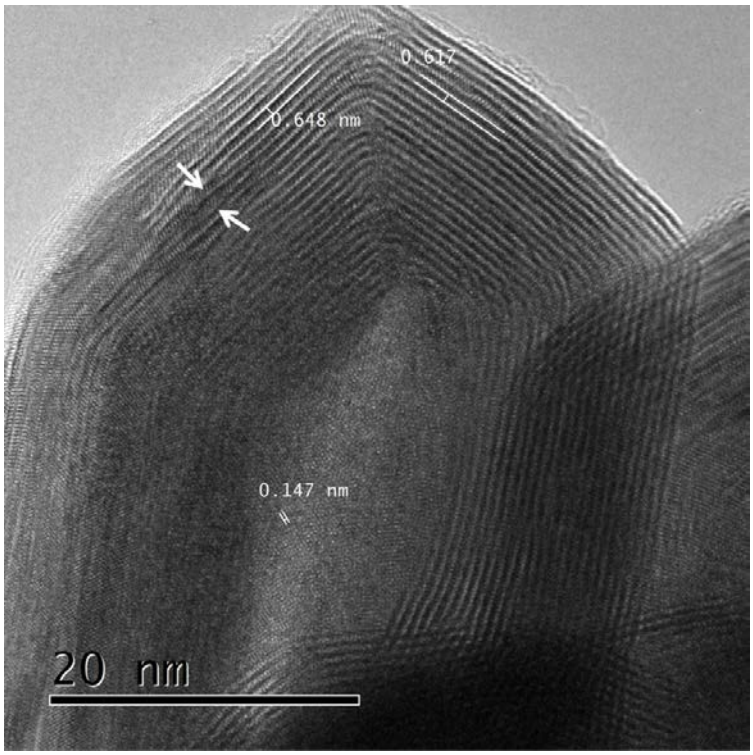

Figure 6. TEM image of the hydrogenated IF-WS_2 NP. The arrows show the expansion of the interlayer spacing up to 0.85 nm.

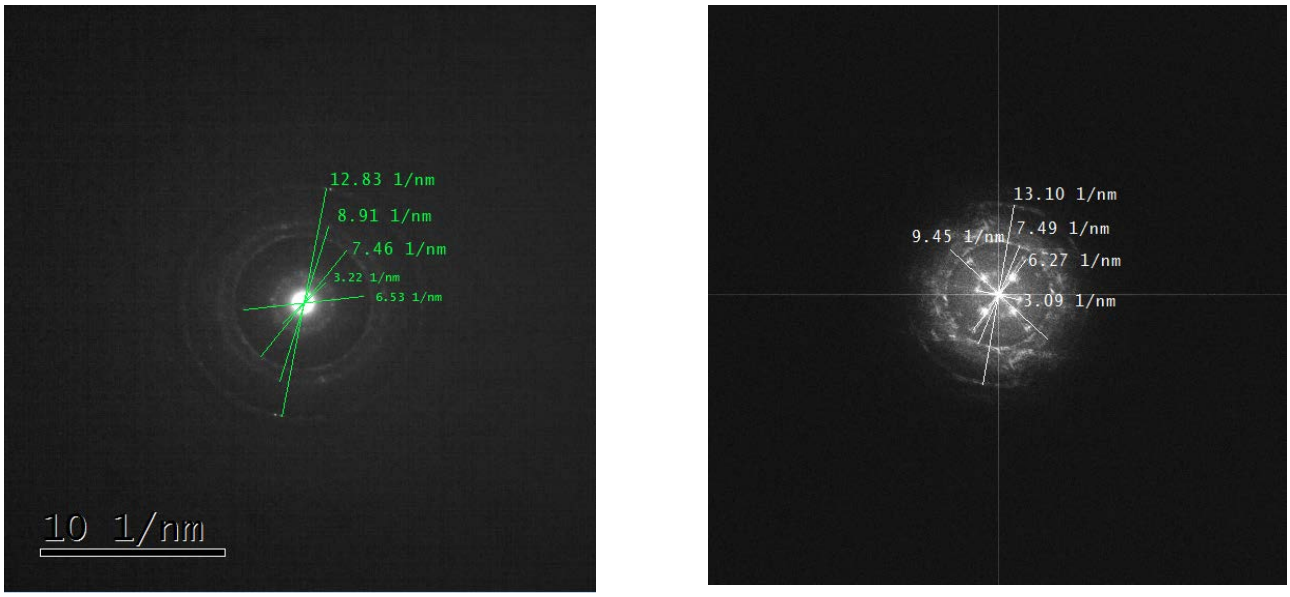

Figure 7. Electron diffraction pattern of the reference (left) and hydrogenated (right) IF-WS_2 NP.

DFT modeling of the hydrogen configuration and adsorption sites

Density functional theory (DFT) calculations have been performed to model the adsorption of hydrogen on planar and curved layered WS_2 nanostructures.[26] These calculations help in the interpretation of the experimental results presented above. The Perdew-Burke-Ernzerhof (PBE) functional has been used for electronic exchange and correlation effects,[27] and van der Waals interactions have been included through the perturbative DFT+D formalism of Grimme.[28] Periodic boundary conditions were applied to model the infinite WS_2 planar layer, the trilayer, the surface and the bulk crystal. The Brillouin zone for all the layered systems was sampled by means of a [4×4×1] Monkhorst-Pack grid,[29] guaranteeing full convergence in energy and electronic density. In the (4×4) unit cell of all the layered systems considered, the unit cell in each WS_2 layer, with a calculated size of 12.6×12.6 $Å^2$, contains 48 atoms, showing perfect WS_2 stoichiometry. The calculated inter-layer distances are 6.13 Å for the case of the trilayer, and 6.15 Å for the bulk. In the surface case, the optimized distance between layers near the surface is 6.14 Å. It should be noticed that the predicted interlayer distance in the bulk is in good agreement with the experimental value of 6.23 Å,[30] the deviation being only 1.2 %.

We have also investigated a variety of WS_2 NT: arm-chair and zig-zag single-walled NT, and (10,10)@(16,16) and (20,0)@(32,0) double-walled (DW) NT. The calculated distance between the inner and the outer walls in the DW-NT is 6.21 Å, slightly larger than the interlayer distances for planar multilayers (6.15 Å). This result is consistent with the experimental one,[31] because the spacing between layers in multiwall NT was found to be 6.31 Å as compared to 6.23 Å in the bulk, and was attributed to the elastic strain. Comparison of the calculated interlayer distances in NT, 6.21 Å, with the experimental value of 6.31 Å shows a deviation of 1.6 %. Although the theoretical and experimental spacing values show small differences, the relative changes are in good agreement. To test the robustness of the structures obtained, and their thermal stability, DFT molecular-dynamics simulations were carried out by heating some NT up to 850 °C, and the structures were found to be stable.

Table 1. Adsorption energies E_{ads} per H_2 molecule, and adsorption distances d_{ads}, for adsorption configurations I and II. The results are the same for the WS_2 layer, the trilayer, and the surface.

	Configuration I		Configuration II	
H_2 coverage	E_{ads} (eV)	d_{ads} (Å)	E_{ads} (eV)	d_{ads} (Å)
0.0625 ML	0.06	2.83	0.07	2.95
0.25 ML	0.06	2.84	0.07	2.96
0.5 ML	0.06	2.84	0.06	2.96
1 ML	0.05	2.86	0.06	2.98

The calculations of the adsorption of molecular hydrogen on the surface of different layered WS_2 structures reveal two preferential adsorption configurations with similar adsorption energies: H_2 molecules on top of a W atom, with the molecular axis lying parallel to the surface (configuration I) and perpendicular to the surface (configuration II). In these adsorption configurations, a triangular hollow formed by three S atoms permits the accommodation of physisorbed H_2 molecules. The H_2 adsorption energies and distances have been monitored as a function of H_2 coverage, ranging between 0.0625 monolayers (ML) coverage (one H_2 molecule per unit cell; the WS_2 unit cell has 48 atoms or 16 molecules) up to full 1 ML coverage (16 H_2 molecules per unit cell or one H_2 molecule per WS_2 molecule). The results for planar layered substrates are given in Table 1, where d_{ads} is the adsorption distance between the center of mass of the H_2 molecule and the plane of S atoms. The results are the same for the WS_2 layer, the trilayer, and the surface.

Table 2. Adsorption energies E_{ads} per molecule and adsorption distances d_{ads} for the most stable H_2 adsorption configurations (I and II, as in Table 1) on the external surface of WS_2 DW-NT. The coverage is low, one molecule adsorbed per NT unit cell.

NT	Configuration I		Configuration II	
	E_{ads} (eV)	d_{ads} (Å)	E_{ads} (eV)	d_{ads} (Å)
(10,10)@(16,16)	0.06	2.83	0.07	2.95
(20,0)@(32,0)	0.06	2.84	0.06	2.96

The adsorption energies are positive; that is, molecular adsorption is favorable. As the H_2 coverage increases, adsorption energies tend to decrease and adsorption distances tend to increase, although these changes are small. A relevant result is that the H_2 adsorption on the topmost layer of the WS_2 multilayers (trilayer and surface) induces a small increase of the distance between the topmost and the second WS_2 layers, and this decoupling is enhanced by increasing the H_2 coverage: the interlayer distances of 6.13 and 6.14 Å for the clean WS_2 trilayer and the surface, respectively, increase up to values of 6.21 and 6.23 Å, respectively, for 1 ML coverage. Another interesting observation is that the strength of the adsorption energies is similar to that on graphene.[32,33]

Similar conclusions are obtained for DW-NT. The results reported in Table 2 correspond to low coverage of the outermost wall of the NT, one adsorbed molecule per NT unit cell. For H_2 adsorption on the innermost wall of the DW-NT, that is, on the hollow internal surface, the adsorption energies are practically the same as for adsorption on the external walls. However, a slight increase in the adsorption distances is observed. By increasing the H_2 content (up to 0.5 ML) for external and internal adsorption, no significant changes are found compared to the case of the planar layers.

The calculations indicate that molecular hydrogen can be adsorbed on the surface of the NP and on the outermost and innermost walls of the NT. However, intercalation between the WS_2 layers is unfavorable. This conclusion has been obtained by simulating the intercalation of the trilayer with increasing amounts of molecular hydrogen; more specifically, H_2 molecules were placed in between the first and second layers of the trilayer (see Figure 8).

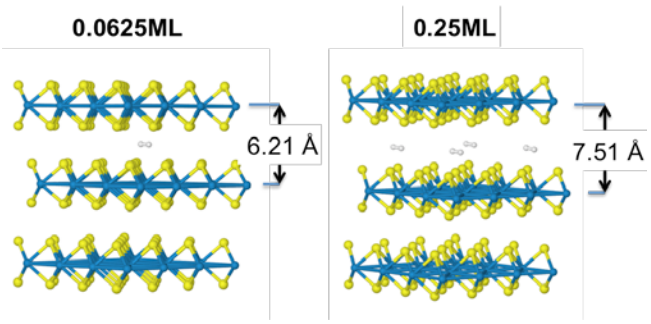

Figure 8. Optimal structures for intercalation of molecular hydrogen between the first and the second layers of the WS_2 trilayer: 0.0625 ML H_2 content (left panel); 0.25 ML H_2 content (right panel).

Table 3 summarizes the intercalation energy per molecule and the distance between the first and the second WS_2 layers, as a function of intercalate concentration. The calculations revealed that the distance between the first and the second layers increases substantially as the hydrogen content increases, from 6.21 Å in the case of no intercalation to values close to 8.6 Å for intercalation of a full hydrogen monolayer. The energy of intercalation is negative in all cases; that is, intercalation is unfavorable due to the elastic energy needed to expand the interlayer distances. Interestingly, an interlayer expansion up to 9 Å in some regions was revealed in the TEM micrographs (Figure 6). Such an expansion was never observed in virgin WS_2 NP. Consequently, the observed interlayer expansion can be interpreted as indicating that some molecular hydrogen intercalates in the NP under the plasma conditions, albeit inducing substantial local distortions on the IF structure. In fact, we find no other mechanism able to explain a local increase in the interlayer distances so large (more than 30%), and at the same time so close to the DFT prediction. Such a substantial expansion can only be due to stuffing some material between the WS_2 layers. The plasma conditions provide the energy required for the H_2 molecules to intercalate in the following way: In the plasma formed sheath on the surface of the sample, the plasma ions are accelerated by the potential drop of ~$3T_e$, where T_e is the electron temperature: ~2 eV in the conditions similar to those used by us.[34] These accelerated ions collide with neutrals and form an energetic mixture of ions-neutrals flowing toward the simple surface.

Table 3. Distance between the first and the second layers, $d_{L1\text{-}L2}$, and intercalation energy per molecule, E_{int} /H_2, for intercalation of molecular hydrogen between the first and the second layers of the WS_2 trilayer. Results are given for several H_2 concentrations.

H_2 content	$d_{L1\text{-}L2}$ (Å)	E_{int}/H_2 (eV)
0.0625 ML	6.21	-2.34
0.25 ML	7.51	-1.01
0.5 ML	8.17	-0.48
1 ML	8.61	-0.19

The concentration of stored hydrogen achieved in the RF experiments, estimated from the TGA measurements, is 0.4-0.55 wt.%. How those concentrations can be understood with the help of the DFT model calculations, considering that only the outer layers and the hollow cores could adsorb molecular hydrogen? By taking the simplest model of a single WS_2 layer with one side of the layer fully covered by H_2 (1 ML), the concentration of hydrogen is 0.81 wt.%. But, for 1 ML of H_2 on the upper surface of the WS_2 bilayer the concentration decreases to 0.40 wt.%, to 0.27 wt.% for a trilayer, and so on. In other words, the hydrogen concentration decreases quickly for n-layer systems, and the same occurs for multiwall NT. Consequently, additional adsorption mechanisms are required to explain the measured adsorption.

One plausible mechanism is that the plasma conditions force the intercalation of some molecular hydrogen, locally distorting the structure of the nanoparticles, as discussed above. The effects of that forced intercalation become reflected in the regions showing increased interlayer distances detected by TEM (see Figure 6).

Another plausible method to obtain higher hydrogen concentration could be H_2 adsorption on planar-like nanostructures and “small” INT (single- to five-layered nanotubes) formed by high power plasma treatment of “big” multiwall INT. Previous work by one of us showed that this occurs when thick WS_2 NP and NT are subject to high-power irradiation.[16] “Daughter” NT and platelets, one to three layers thick, were observed to form in those experiments. In the current study, however, TEM analysis of the powders after plasma treatment did not show evidences for the formation of new morphological structures. The reason can be the

different plasma conditions used in the previous work: higher power of the plasma (600 W) and heavier (Ar) plasma indeed could result in single wall NT formation.

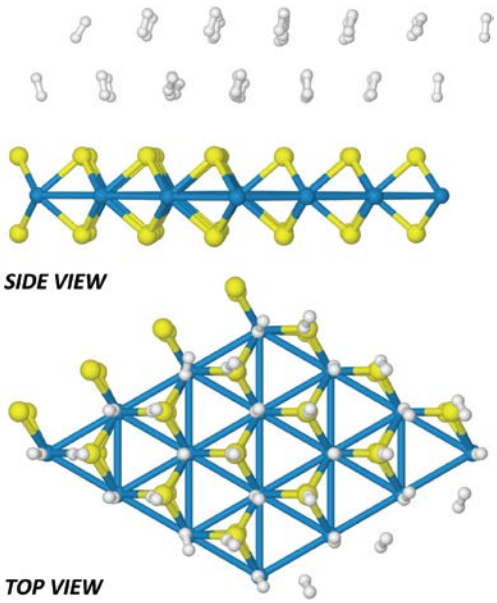

Figure 9. Optimized structure for 2 ML of H_2 molecules adsorbed on top of a WS_2 layer.

A third plausible mechanism is the condensation of more than one hydrogen monolayer on the surface of planar platelets, or on the external surfaces and hollow internal surfaces of NT. As a test, we performed simulations for the covering of a single WS_2 layer with more than 1 ML of H_2. The starting configuration was formed by H_2 molecules on top of all W and S atoms (this corresponds to 2 ML coverage in the notation used above). The molecules were initially on the same plane. But this turns out to be an unfavorable configuration because the H_2 molecules are too close to their neighbor molecules, and structural relaxation of the system allowed the adsorbed molecules to optimize their positions forming 2 ML, as shown in Figure 9. The H_2 layer closest to the WS_2 layer is at a distance of 2.84 Å from the plane of S atoms, and the top H_2 layer is separated from the first one by a distance of 2.52 Å. The molecules of the first layer sit on top of the W atoms, while the positions of the molecules of the top H_2 layer correspond to sites above S atoms. In all cases, the molecular axes are nearly perpendicular to the plane. The calculated adsorption energy, 0.06 eV per molecule, is nearly the same as the adsorption energy per molecule for a single H_2 ML (see Table 1).

Table 4. Distance between the first and second layers, $d_{L1\text{-}L2}$, and intercalation energy per atom, E_{int}/H, for the intercalation of atomic hydrogen between the first and the second layers in the WS_2 trilayer. Results are given as a function of increasing H content.

H content	$d_{L1\text{-}L2}$ (Å)	E_{int} / H (eV)
0 ML	6.14	-
0.25 ML	6.15	1.15
0.5 ML	6.17	1.32
0.75 ML	6.21	1.36
1 ML	6.25	1.38

The mechanisms discussed above are not mutually exclusive, and could add up to explain the amount of stored hydrogen observed in the experiments. In fact, an additional possible mechanism could also be offered. Neutral H atoms and H^+ ions are generated in the RF hydrogen plasma, in addition to molecular hydrogen. Intercalation of atomic hydrogen leads to positive intercalation energies (see Table 4); that is, the intercalated systems are stable. The intercalated H atoms attach to S atoms and induce only a very small increase in the distance between adjacent WS_2 layers, in contrast with the intercalation of molecular hydrogen (compare Tables 3 and 4). However, the Raman experiments performed did not detect H-S (or D-S) bonds, which would reveal the presence of adsorbed atomic hydrogen. So we have to admit that the amount of atomic hydrogen intercalated in between the layers of platelets, IF, and NT is non-significant during the Raman measurements, perhaps because the hydrogen atoms have recombined to form hydrogen molecules, which in turn do not intercalate. In addition, absence of the H-S and D-S bonds related features in the Raman measurements could be a result of desorption under Raman beam heating or even samples aging (time required to transformation of the sample after plasma treatment).

Conclusions

In summary, the configuration and energy states of the hydrogen species adsorbed in the NP of WS_2 were elucidated by using experimental analytical methods and a DFT theoretical model. The micro-Raman spectroscopy detected the H-H and D-D stretching modes at 4150 cm^{-1} and 2970 cm^{-1}, respectively, indicating that the hydrogenation by the RF plasma results in physisorption of molecular hydrogen/deuterium. No evidences of H-S and D-S bonds were found by micro-Raman analysis. The adsorbed hydrogen is found to be quite stable at room temperature conditions, both in air and vacuum. The DFT calculations, for the first time applied to the studied system, show that, the physisorbed hydrogen molecules are adsorbed, probably as one or more layers, on the very surface of the NP (e.g., on the top-most layer and the innermost layer of the hollow NT). DFT calculations performed to analyze the possible intercalation of molecular hydrogen between WS_2 layers delivered insertion energies indicating that such intercalation is unfavorable. However, we suppose that partial intercalation of molecular hydrogen could take place under the RF plasma conditions. The forced intercalation causes local damage and a substantial expansion of the interlayer distances, which we have observed by TEM.

On the other hand, DFT calculations for atomic and ionic hydrogen reveal that intercalation would be energetically favorable. No direct evidence was found for intercalation of atomic hydrogen since it may have followed either or both processes: de-intercalation and shrinking caused by environmental affects before being measured by micro-Raman. Additional studies are required for identification of possible intercalation of atomic hydrogen.

The results obtained by the DFT calculations can be used now for further optimization of hydrogen exposure conditions, e.g., using plasma with higher concentration of atomic and ionic hydrogen, and lowering the temperature of the RF-plasma enhanced process to intensify the adsorption process. In addition, as the adsorption of molecular hydrogen is found to be favorable on the very surface, single wall NT can be used instead to increase the hydrogen weight percent.

Acknowledgments: This work was partially supported by the Israel-Korea grant of Israeli and Korean governments, by ENIAC European grant “Lab4MEMS” Nr. ENIAC 3 /2013-UEFISCDI, and by European

COST actions MP1103, MP1302, and CM1301. The work of JAA was supported by MINECO (grant MAT2014-54378-R) and Junta de Castilla y León (grant VA050U14). JIM acknowledges funding from the ERC Synergy Grant ERC-2013-SYG-610256 NANOCOSMOS, and computing resources from CTI-CSIC. AZ acknowledges the support provided by the INNI-FTA grant and Pazy foundation. The authors thank Amnon Fruchtman (Plasma Lab., HIT) for helpful discussion of the RF plasma exposure experiments and analysis of the pressure curves.

References

1. Feldman, Y.; Zak, A; Popovitz-Biro, R; Tenne, R. New Reactor for Production of Tungsten Disulfide Hollow Onion-Like (Inorganic Fullerene-Like) Nanoparticles. *Solid State Sci.* **2000**, *2*, 663-672.

2. Zak, A.; Sallacan-Ecker, L.; Margolin, A.; Feldman, Y.; Popovitz-Biro, R.; Albu-Yaron, A.; Genut, M.; Tenne, R. Scaling Up of the WS_2 Nanotubes Synthesis. *Fuller. Nanotub. Car. N.* **2010**, *19*, 18-26.

3. Laikhtman, A.; Michaelson, S.; Hoffman, A.; Kim. T. K.; Moon, H. R.; Zak, A. Using Hydrogen Activated by Microwave Plasma vs. Molecular Hydrogen for Hydrogen Storage in Tungsten Disulfide Inorganic Nanotubes. *Int. J. Hydrogen Energ.* **2014**, *39*, 9837-9841.

4. Cacciatore, M.; Rutigliano, M. Dynamics of Plasma–Surface Processes: E–R and L–H Atom Recombination Reactions. *Plasma Sources Sci. Technol.* **2009**, *18*, 023002.

5. Nishijima, D.; Sugimoto, T.; Iwakiri, H.; Ye, M. Y.; Ohno, N.; Yoshida, N.; Takamura, S. Characteristic Changes of Deuterium Retention on Tungsten Surfaces due to Low-Energy Helium Plasma Pre-Exposure. *J. Nucl. Mater.* **2005**, *337-339*, 927-931.

6. Glazunov, G. P.; Andreev, A. A.; Baron, D. I.; Causey, R. A.; Hassanein, A.; Kitayevskiy, K. M.; Konotopskiy, A. L.; Lapshin, V. I.; Neklyudov, I. M.; Patokin, A. P.; *et al.* Hydrogen Permeability and Erosion of W-Pd Bimetallic Systems. *Fusion Eng. Des.* **2006**, *81*, 375-380.

7. Ross, D. J.; Halls, M. D.; Nazri, A. G.; Aroca, R. F. Raman Scattering of Complex Sodium Aluminum Hydride for Hydrogen Storage. *Chem. Phys. Lett.* **2004**, *388*, 430-435.

8. Wesełucha-Birczyńska, A.; Babeł, K.; Jurewicz, K. Carbonaceous Materials for Hydrogen Storage Investigated by 2D Raman Correlation Spectroscopy. *Vib. Spectrosc.* **2012**, *60*, 206-211.

9. Mosquer, E.; Diaz-Droguett, D. E.; Carvajal, N.; Roble, M.; Morel, M.; Espinoza, R. Characterization and Hydrogen Storage in Multi-Walled Carbon Nanotubes Grown by Aerosol-Assisted CVD Method. *Diam. Relat. Mater.* **2014**, *43*, 66-71.

10. Panella, B.; Hirscher, M. Raman Studies of Hydrogen Adsorbed on Nanostructured Porous Materials. *Phys. Chem. Chem. Phys.* **2008**, *10*, 2910-2917.

11. Gartsman, K.; Kaplan-Ashiri, I.; Tenne, R.; Rafailov, P. M.; Thomsen, C. Micro Raman Investigation of WS_2 Nanotubes. *AIP Conf. Proc.* **2005**, *786*, 349-352.

12. Rafailov, P. M.; Thomsen, C.; Gartsman, K.; Kaplan-Ashiri, I.; Tenne, R. Orientation Dependence of the Polarizability of an Individual WS_2 Nanotube by Resonant Raman Spectroscopy. *Phys.Rev. B* **2005**, *72*, 205436.

13. Schuffenhauer, C.; Wildermuth, G.; Felsche, J.; Tenne, R. How Stable are Inorganic Fullerene-Like Particles? Thermal Analysis (STA) of Inorganic Fullerene-Like NbS_2, MoS_2, and WS_2 in Oxidizing and Inert Atmospheres in Comparison with the Bulk Material. *Phys. Chem. Chem. Phys.* **2004**, *6*, 3991-4002.

14. Feldman, Y.; Frey, G. L.; Homyonfer, M.; Lyakhovitskaya, V.; Margulis, L.; Cohen, H.; Hodes, G.; Hutchison, J. L.; Tenne, R. Bulk Synthesis of Inorganic Fullerene-Like MS_2 (M = Mo, W) from the Respective Trioxides and the Reaction Mechanism. *J. Am. Chem. Soc.* **1996**, *118*, 5362-5367.

15. Feldman, Y.; Lyakhovitskaya, V.; Tenne, R. Kinetics of Nested Inorganic Fullerene-Like Nanoparticle Formation. *J. Am. Chem. Soc*. **1998**, *120*, 4176-4183.

16. Brüser, V.; Popovitz-Biro, R.; Albu-Yaron, A.; Lorenz, T.; Seifert, G.; Tenne, R.; Zak, A. Single- to Triple-Wall WS_2 Nanotubes Obtained by High-Power Plasma Ablation of WS_2 Multiwall Nanotubes. *Inorganics* **2014**, *2*, 177-190.

17. Laikhtman, A.; Hoffman, A. Laser Power Effects on the Raman Spectrum of Isolated Diamond Chemical Vapor Deposition Particles. *J. Appl. Phys.* **1997**, *82*, 243-248.

18. Baserga, A.; Russo, V.; Di Fonzo, F.; Bailini, A.; Cattaneo, D.; Casari, C. S.; Li Bassi, A.; Bottani, C. E. Nanostructured Tungsten Oxide with Controlled Properties: Synthesis and Raman Characterization. *Thin Solid Films* **2007**, *515*, 6465-6469.

19. Hartwig, C. M.; Vitko, J., Jr. Raman Spectroscopy of Molecular Hydrogen and Deuterium Dissolved in Vitreous Silica. *Phys. Rev. B* **1978**, *18*, 3006-3014.

20. Schmidt, B. C.; Holtz, F. M.; Bény, J. –M. Incorporation of H_2 in Vitreous Silica, Qualitative and Quantitative Determination from Raman and Infrared Spectroscopy. *J. Non-Cryst. Solids* **1998**, *240*, 91-103.

21. Thompson, S. D.; Carroll, D. G.; Watson, F.; O'Donnell, M.; McGlynn, S. P. Electronic Spectra and Structure of Sulfur Compounds. *J. Chem. Phys.* **1966**, *45*, 1367-1379.

22. Zak, A.; Feldman, Y.; Lyakhovitskaya, V.; Leitus, G.; Popovitz-Biro, R.; Wachtel, E.; Cohen, H.; Reich, S.; Tenne, R. Alkali Metal Intercalated Fullerene-Like MS(2) (M = W, Mo) Nanoparticles and Their Properties. *J. Am. Chem. Soc.* **2002**, *124*, 4747-4758.

23. Centrone, A.; Siberio-Perez, D. Y.; Millward, A. R.; Yaghi, O. M.; Matzger, A. J.; Zerbi, G. Raman Spectra of Hydrogen and Deuterium Adsorbed on a Metal–Organic Framework. *Chem. Phys. Lett.* **2005**, *411*, 516-519.

24. Anderson, A.; Binbrekt, S.; Tang, H. C. Raman and Infrared Study of the Low Temperature Phase of Solid H_2S and D_2S. *J. Raman Spectrosc.* **1977**, *6*, 213-220.

25. Sakashita, M.; Fujihisa, H.; Yamawaki, H.; Aoki, K. Molecular Dissociation in Deuterium Sulfide under High Pressure: Infrared and Raman Study. *J. Phys. Chem. A* **2000**, *104*, 8838-8842.

26. Baroni, S.; Corso, A. D.; Gironcoli, S.; Giannozzi, P. *QUANTUM ESPRESSO Package* **2005**, in www.quantum-espresso.org.

27. Perdew, J. P.; Burke, K.; Ernzerhof, M. Generalized Gradient Approximation Made Simple. *Phys. Rev. Lett.* **1997**, *78*, 3865-3868.

28. Grimme, S. J. Semiempirical GGA-Type Density Functional Constructed with a Long-Range Dispersion Correction. *J. Comput. Chem.* **2006**, *27*, 1787-1799.

29. Monkhorst, H. J.; Pack, J. D. Special Points for Brillouin-Zone Integrations. *Phys. Rev. B* **1976**, *13*, 5188-5192.

30. Wilson, J. A.; Yoffe, A. D. The Transition Metal Dichalcogenides Discussion and Interpretation of the Observed Optical, Electrical and Structural Properties. *Adv. Phys.* **1968**, *18*, 193-335.

31. Zak, A.; Sallacan-Ecker, L.; Margolin, A.; Genut, M.; Tenne, R. Insight into the Growth Mechanism of

WS_2 Nanotubes in the Scaled-Up Fluidized Bed Reactor. *Nano* **2009**, *4*, 91-98.

32. Cabria, I.; López, M. J.; Alonso, J. A. The Optimum Average Nanopore Size for Hydrogen Storage in Carbon Nanoporous Materials. *Carbon* **2007**, *45*, 2649-2658.

33. Cabria, I.; López, M. J.; Alonso, J. A. Hydrogen Storage Capacities of Nanoporous Carbon Calculated by Density Functional and Møller-Plesset Methods. *Phys. Rev. B* **2008**, *78*, 075415.

34. Geng, Z. C.; Xu, Y.; Yang, X. F.; Wang, W. G.; Zhu, A. M. Atomic Hydrogen Determination in Medium-Pressure Microwave Discharge Hydrogen Plasmas via Emission Actinometry. *Plasma Sources Sci. Technol.* **2005**, *14*, 76-82.

TOC Graphic

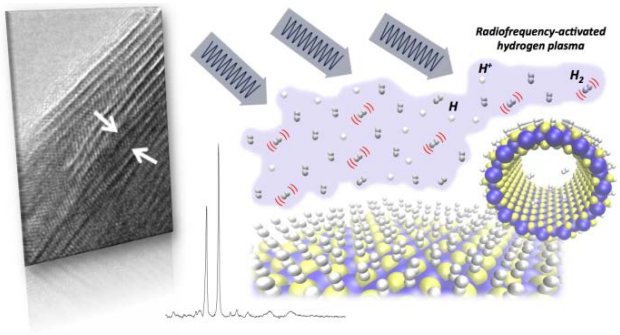

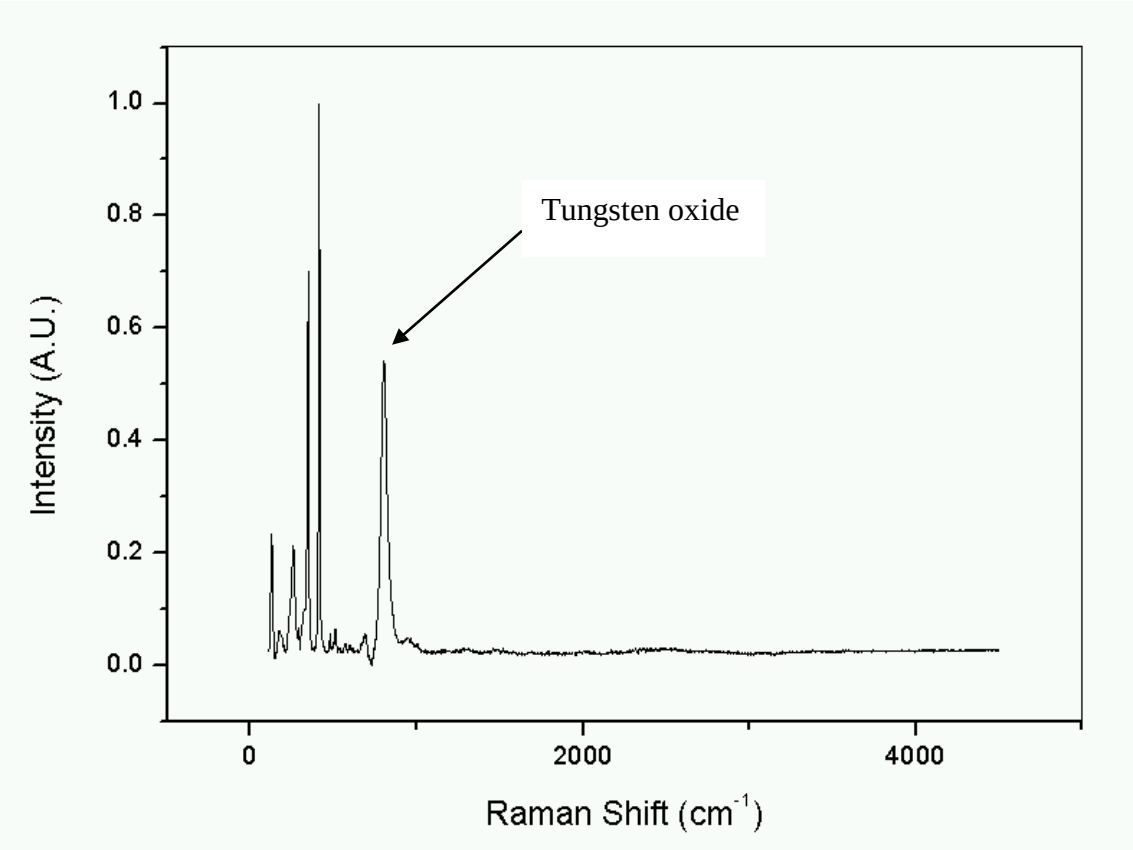

Micro-Raman spectra of WS_2 NP measured using 500 mW power laser beam – for reviewer only.

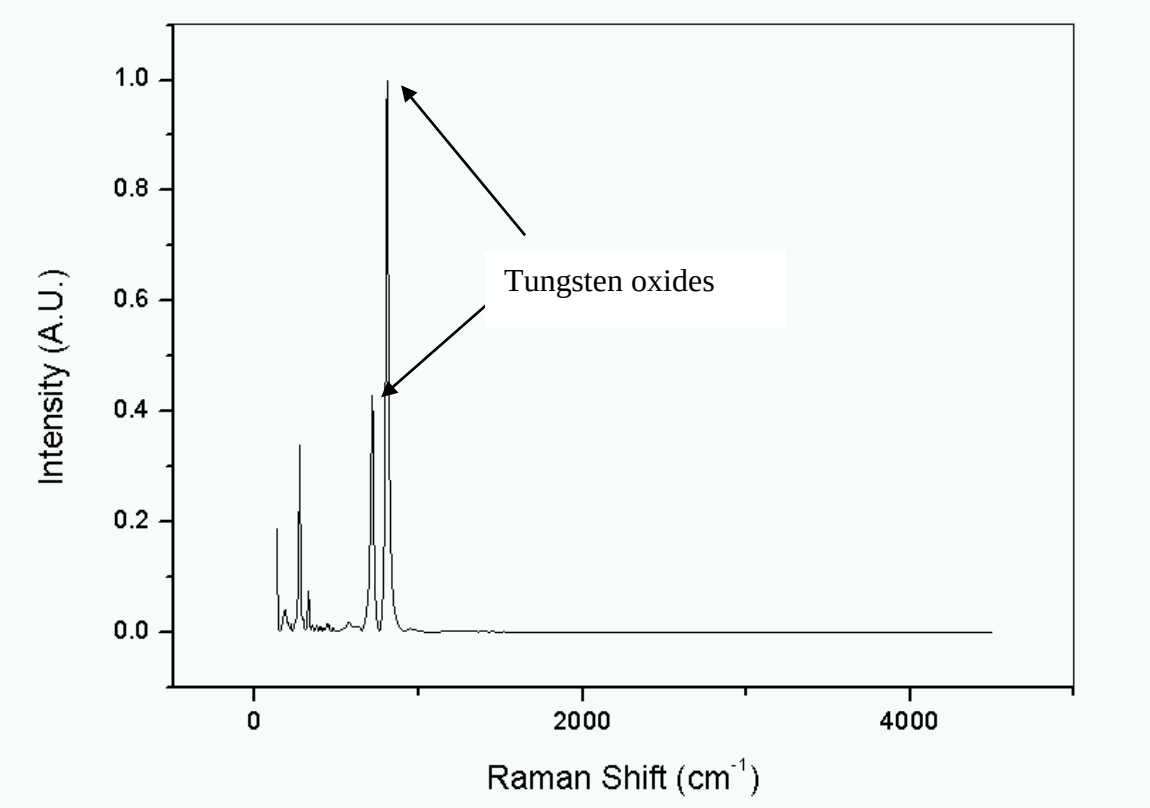

Micro-Raman spectra of WS_2 NP measured using 800 mW power laser beam – for reviewer only.

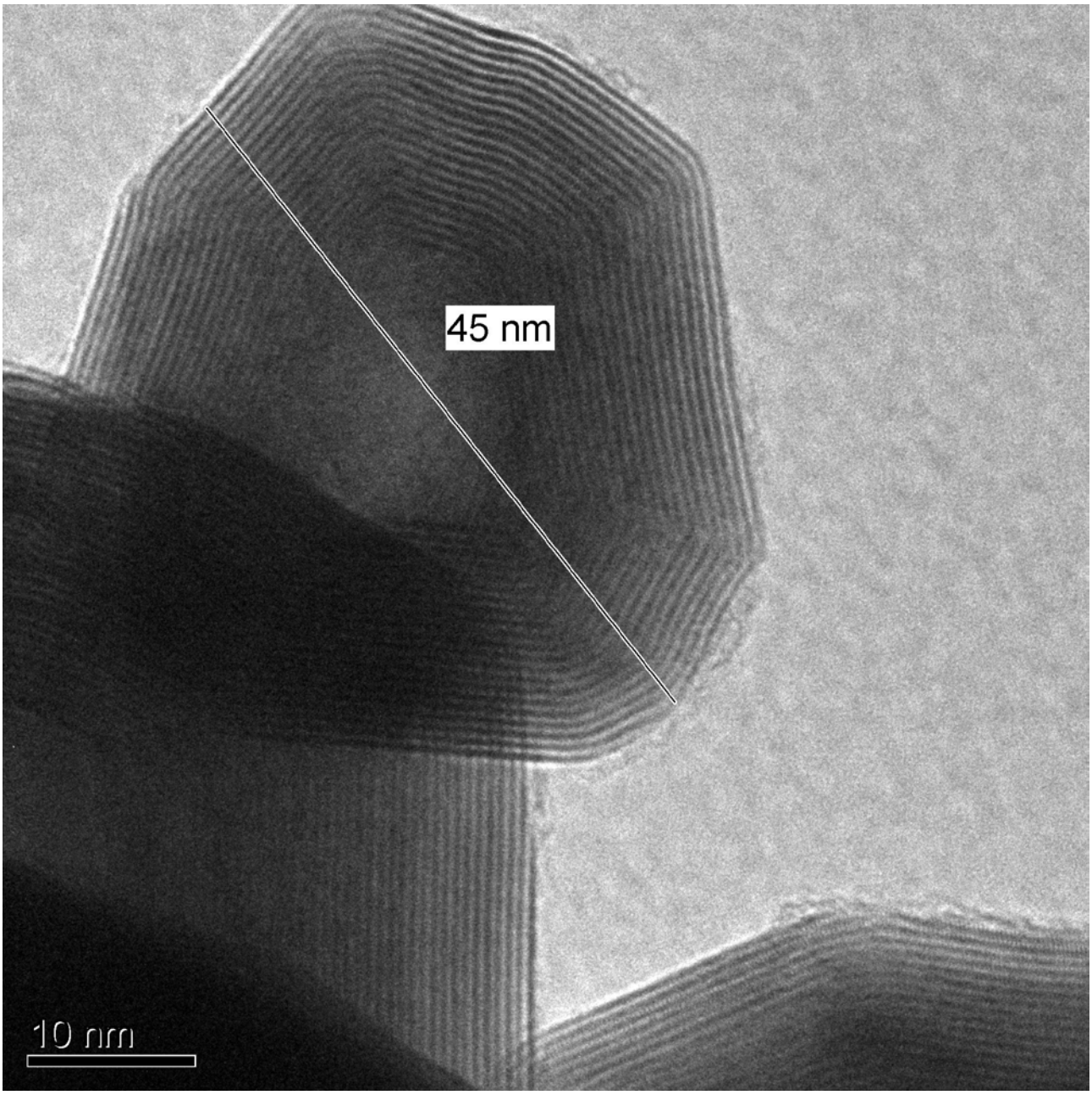

TEM image of pristine WS_2-IF - for reviewers only.